5 Exozodiacal Disks

Phil Hinz, University of Arizona, Chair

Rafael Millan-Gabet, NASA Exoplanet Science Institute, Co-Chair

Olivier Absil, Rachel Akeson, David Ardila, James Breckenridge, Geoffrey Bryden, Christine Chen, David Ciardi, Mark Clampin, Vincent Coudé du Foresto, William Danchi, Denis Defrère, Dennis Ebbets, Sally Heap, John Krist, Marc Kuchner, Charles Lillie, Patrick Lowrance, Stanimir Metchev, Rafael Millan-Gabet, Marshall Perrin, Meyer Pesenson, Peter Plavchan, Sam Ragland, Stephen Rinehart, Aki Roberge, Chris Stark, Karl Stapelfeldt, Motohide Tamura, Angelle Tanner, Neal Turner, Bruce Woodgate

5.1 Introduction

Characterization of the debris disks around nearby stars is an important complement to planet finding for several reasons. Primarily, the detection of debris material, especially in or close to the habitable zone is a direct indication of planet-building material in this zone. In a gas-poor disk, debris material is cleared away through collisional destruction, radiation pressure, or Poynting-Robertson drag on relatively short timescales compared to those of planet formation or the planetary system itself. Therefore, the presence of dust indicates that larger parent bodies must also be located in the system. Thus, the detection of dust, in tandem with detection of the massive planets in the system allows the development of a more complete observational picture of the architecture of a planetary system. In fact, information gleaned from disk structure can be used to detect planets that would otherwise be too faint or have a mass that is too low to be detected using other techniques. Similarly, the presence of small-body populations in a habitable zone could affect habitability through the frequency of large impact events. However, for the ultimate goal of detecting and characterizing an Earth-like exoplanet, debris disks can decrease the significance of the detection and potentially obscure the planet signal altogether.

The recently completed report by the Exoplanet Task Force made two recommendations related to dust disk detection. In the near term (1–5 years) they recommended the community "invest in a census of exozodi systems around exoplanet target stars," and in the medium term (6–10 years) that the community should "implement next generation high spatial resolution imaging techniques on ground-based telescopes: AO for direct detection of young, low-mass companions, and interferometry for disk science."

This chapter describes the state of the field and near future plans for exozodiacal dust detection and modeling. The plans described in the chapter agree substantially with those of the ExoPlanet Task Force. Based on discussion in the May 2008 Exoplanet Forum, following is the consensus set of recommendations on exozodiacal dust:

- ***NASA should continue its support of KI, LBTI, and similar efforts that will measure zodiacal dust density and morphology critical for planning future direct-imaging missions***
- ***Continue studies of Exoplanet Probe-class space missions that can address the density and morphology of dust in the habitable zone of nearby stars with a much higher sensitivity limit and a much larger sample of nearby systems than can be done with ground-based technologies.***
- ***Continue the development of collisional debris disk models to complement observations, aiding in interpretation and extrapolation of such results.***

5.1.1 Properties of Protoplanetary and Exozodiacal Disks

During the collapse of dense interstellar cloud cores, conservation of angular momentum dictates the formation of a rotating disk of gas and dust around the young star. Planets grow in this circumstellar disk, interact with it, and implant their signatures on it. The discovery of such disks around nearby stars has provided the opportunity to study planet formation in real time, rather than working backward from completed or mature systems. It is now understood that planet formation is a general physical process that operated in our own young Solar System, including the transformation of interstellar organic material into pre-biotic compounds like those that gave rise to life on Earth. The older, dust-rich disks—debris disks—are also vital for efforts to image and characterize extrasolar terrestrial planets. Debris dust surrounds our Sun today (the zodiacal dust) and about 10–20% of nearby stars harbor a currently detectable debris disk, typically detected at a separation similar to the Sun's Kuiper belt (e.g., Beichman et al. 2006; Trilling et al. 2008; Hillenbrand et al. 2008) but the extension of these statistics to the habitable zone is not yet known. While exozodiacal dust is a major source of background flux and probably confusion in direct imaging of exoplanets, it may also provide indirect evidence of planets through dust structures caused by gravitational perturbations. The signature of the Earth may be seen in clumps within the zodiacal dust in the inner Solar System.

The current paradigm for the formation of a mature planetary system has three main phases:

- Formation of gas-giant planets like Jupiter,
- Formation of terrestrial planets, and
- Clearing of most leftover planetesimals (i.e. asteroids & comets) from the system.

This timeline is represented in Figure 5-1. It is during the last phase that most of the volatile content of Earth's surface was delivered by the impact of water-rich planetesimals (e.g., Morbidelli et al. 2000). Protoplanetary disks may be divided into three classes that appear to roughly correspond to each phase.

1. The youngest class is the *primordial disks*, which are composed of relatively unprocessed interstellar material left over from star formation. Primordial disks are gas-rich, as evidenced by observations of sub-mm CO emission (e.g., Thi et al. 2000); the bulk of the gas, however, is molecular hydrogen. Since giant planets are primarily composed of gas, they must form in gas-rich disks, and the primordial disks match this description. Contrary to earlier conception, these disks are apparently not quiescent or static. They are the sites of active chemistry and large-scale motions of gas, dust, and planetary bodies of all sizes through migration.

2. The next class is the *transitional disks*, which appear to be clearing material from their inner disks, but still retain optically thick, gas-rich outer disks. This relatively new class has been the focus of recent intensive study, as they provide a window on the rapid transformation from a primordial disk into a young planetary system.
3. The oldest class is the *debris disks*, which are dusty, gas-poor disks. These disks are composed of material produced by the destruction of planetesimals and contain little or no unprocessed interstellar material. Debris disks have a wide range of ages, from about 10 Myr to a few Gyr. Terrestrial planets are likely forming in the younger debris disks, while the older ones correspond to the disk-clearing phase. Dust is removed from debris disks through Poynting-Robinson drag, planetary sweeping, or radiation pressure and replenished via collisions between and evaporation of planetesimals.

A coronagraphic image of a disk from each of the three classes appears in Figure 5-1, which implies a very clean, orderly progression in both planet formation and disk evolution. However, the theoretical stages in planet formation may be occurring simultaneously in different parts of a disk. In addition, the different classes of disk are not cleanly separated, with apparent overlap in the age ranges of each class, indicating that stochastic processes may significantly shape the evolutionary pathways of individual systems. The relationship of this diversity of disk properties with the wide range of extrasolar planetary systems remains a topic of current study.

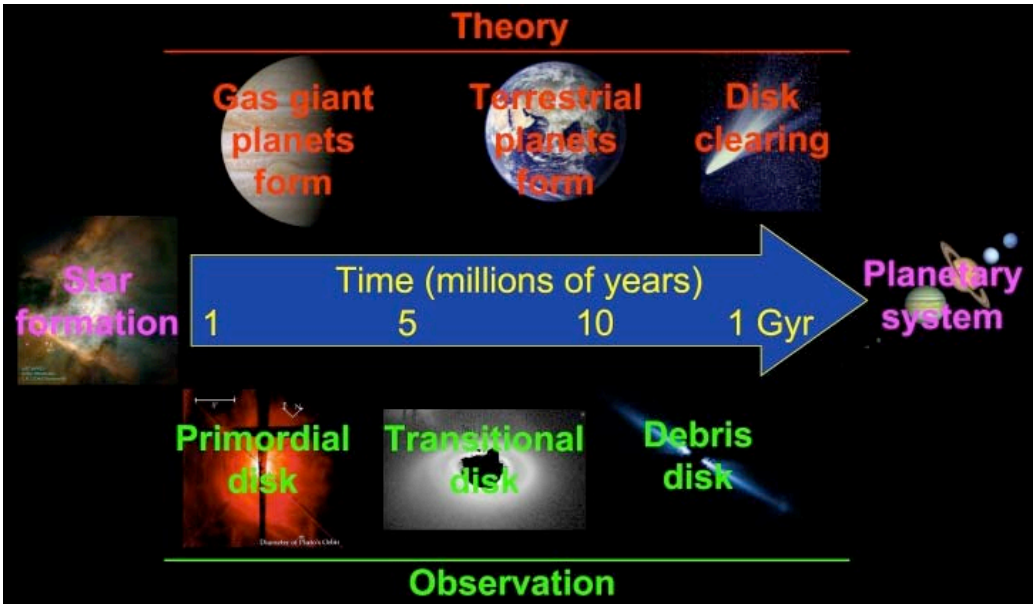

Figure 5-1. Timeline for planet formation and the evolution of circumstellar disks. Above the arrow, the main theoretical phases in planetary formation are shown. Below, the classes of circumstellar disks are identified. A coronagraphic image of an example from each class is shown; the primordial disk around AB Aurigae at left (Grady et al. 1999), the transitional disk around HD 141569A in the center (Clampin et al. 2003), and the debris disk around AU Microscopii at right (Krist et al. 2005). [Figure credit: A. Roberge]

5.1.2 Terrestrial Planet Formation and Delivery of Volatiles

In order for terrestrial-sized planets to acquire large quantities of volatiles such as water, giant planets are likely required to gravitationally stir up planetesimals and inject them into the inner disk. The gas composition in a debris disk may provide information on the composition of the planetesimals producing the disk. For example, recent far-ultraviolet spectroscopy of the gas in the well-studied β Pic debris disk has shown that carbon is extremely overabundant relative to every other measured element (e.g., C/O = 18 × solar; Roberge et al. 2006), despite the fact that the central star appears to have solar metallicity (Holweger et al. 1997). This overabundance likely reflects the composition of the parent material of the gas, which would have to be much more carbon-rich than expected based on what we know about Solar System asteroids and comets. Either the β Pic planetesimals producing the gas are selectively losing their volatile carbon compounds, or they are simply more carbon-rich overall than any Solar System planetesimal. The latter possibility has important consequences for any terrestrial planets that might be forming around β Pic and their volatile composition.

5.1.3 Science Goals

The extrasolar planetary systems already discovered show a surprising diversity in their architectures compared to our own Solar System. Studies of protoplanetary and debris disks are essential to understand the origins of this diversity and to predict what other phenomena might be observed in the future. They also affect our ability to make new discoveries, through the impact of exozodiacal dust on direct imaging and characterization of exoplanets. The primary goals of protoplanetary and debris disk studies are as follows.

Obtain a better understanding of planet formation as a generic and robust process

Planets can form around normal stars with spectral types ranging from at least late M (Butler et al. 2004) to early A (Johnson et al. 2007), around pulsars (e.g., Wolszczan & Frail 1992), and possibly even around brown dwarfs (Chauvin et al. 2004). Their birth environments are apparently also diverse, ranging from low-mass star-forming regions like the Taurus cloud to energetic, high-mass star-forming regions like the Orion nebula. Most planet formation models were developed to explain the Solar System itself and currently cannot explain the diversity of planets already detected. Theoretical improvements to these models are hampered by a lack of basic information on protoplanetary disks, including initial masses of the disks, typical lifetimes of disks around stars of different masses and in different stellar environments, the evolution of the gas-to-dust ratio, density and temperature structure, and chemical evolution. It is highly desirable that models of planet formation be improved so that they would be able to predict the prevalence of Earth-mass planets around different types of stars including ones of varying metallicity and mass, and the predicted abundances of volatile chemicals on their surfaces, to motivate and guide future efforts to find and characterize potentially habitable Earth-like exoplanets.

Characterize the exozodiacal dust around targets for direct imaging of exoplanets

When viewed from a distance, the most conspicuous feature of the Sun's planetary system is the zodiacal dust, which is tenuous but covers a large surface area. A significant fraction of

nearby stars has similar dust at much higher abundance. Emission from exozodiacal dust is likely to be the largest source of astrophysical noise in direct imaging and characterization of exoplanets. If the dust is too bright, the observation time needed to detect and characterize a planet becomes prohibitively long. For the TPF-C mission, the break point was estimated to be 10 times the level of dust in the Solar System (10 "zodis"). In Section 5.1.4, we present a simple prescription for the acceptable levels of exozodi as a function of telescope aperture size. In Sections 5.2 and 5.3, we discuss the current exozodi detection limits and upcoming opportunities to push down to the levels of dust relevant for direct-imaging missions.

Use disk structure to infer the presence of unseen planets

While exozodiacal dust hampers direct imaging of exoplanets, it may also provide another means of indirect detection. In the Solar System, the gravitational influence of the Earth temporarily traps zodiacal dust into a ring at 1 AU, with additional clumps leading and trailing the planet (Dermott et al. 1994). Rings, clumps, and warps (or "x-patterns") have been seen in coronagraphic images of nearby debris disks (e.g., HR4796, Schneider et al. 1999; Fomalhaut, Kalas et al. 2005). Such structures are often attributed to the influence of an unseen planet orbiting in the debris disk, and may be a unique way of finding planets that are extremely difficult to detect with other indirect techniques, like young planets and planets on wide orbits. Unfortunately, we have not yet been able to associate an observed disk dust structure with a known exoplanet. Part of the problem is the difficulty of detecting planets in the currently known debris disks, which have hundreds to thousands of times more dust than the Solar System. The other part of the problem relates to the dynamical modeling used to interpret dust structures. In Section 5.2, we discuss the current state of these models, near-term improvements, and additional needed development.

5.1.4 Science Requirements for Observations of Terrestrial Planets

The requirements on exozodiacal brightness for a Terrestrial Planet Finder are determined by its impact on the increase in integration time for such a mission. Missions in both the visible (0.5–1 μm) and infrared (6–20 μm) are similarly affected. It is worth reviewing the fundamental noise parameters for these missions to appreciate the effect of a denser extrasolar zodiacal dust cloud. Both calculations below assume that effects from residual starlight such as varying suppression or similar systematics, as well as limitations of detector performance, can be kept below the fundamental Poisson noise from local zodiacal light, exozodiacal light and residual starlight. Similar estimates can be found, for example in Brown (2005) or Beichman et al. (2006).

Impact on an Optical Mission

F For an idealized optical mission, the noise in an optical observation is dominated by the Poisson noise associated with background flux from an exozodiacal disk as well as the background flux from local zodiacal dust. The time required to image a planet at optical wavelengths in the presence of background flux from local zodiacal dust, exozodiacal dust, and unsuppressed starlight is given by

$$t_O = \frac{8}{\pi \Delta \lambda F_0} 10^{0.4\left(2 \cdot m_p\right)} \frac{SNR^2}{D^4 T} \left[\left(1+\mu\right) 10^{-0.4z} \pi \lambda^2 206265^2 \psi^2 + \zeta D^2 10^{-0.4 m_s} \right]$$

where ψ is the size of the focal plane photometric aperture in units of λ/*D*, Δλ the bandwidth, F_0 is the photon flux for zero magnitude, m_s is the stellar magnitude, m_p is the magnitude of the planet, z is the surface brightness of the zodiacal light, λ is the central wavelength of the bandpass, D is the diameter of the telescope aperture, T is the total throughput, SNR is the signal-to-noise, μ is the exozodi brightness in units of zodis, and ζ is the scattered and diffracted light (the "contrast") in the photometric aperture relative to the unsuppressed stellar image. Typical values for these parameters appear in Table 5-1. This equation is appropriate for a background-limited observation such as imaging an Earth-like exoplanet.

Table 5-1. Typical parameter values in the exposure time calculation for direct-imaging missions in the visible and the infrared.

Parameter	Visible Value	IR Value	Comment
Ψ	1.5	–	Image "width"
Δλ	0.11 μm	2 μm	20% bandwidth
F_0	9.5×10^{10} photons sec^{-1} m^{-2} μm^{-1}	5×10^7 photons s^{-1} m^{-2} μm^{-1}	
m_s	5	3.5	Sun at 10 pc
m_p	29.9 mag	19.6	Earth at 1 AU from Sun at 10 pc
Z	23 mag $arcsec^{-2}$	14.2 mag $arcsec^{-2}$	Local Zodiacal brightness
Ez	–	14.6 mag	Exozodiacal integrated flux
λ	5.50×10^{-7} m	1.0×10^{-5} m	
D	4 m	2 m	Element size for IR interferometer
T	0.0864, (0.7087)	0.05	Optical: TPF-C (TPF-O)
SNR	10	10	
B	–	20 m	
ζ	5×10^{-11}	1×10^{-5}	Contrast
S	–	4.6×10^{-9} radians	Sun's diameter at 10 pc

Impact on an IR interferometer mission

For an idealized IR interferometer mission (one not limited by systematic errors or noise associated with chopping or nulling), the calculation is similar to the optical mission. The limiting noise sources are the local zodiacal dust emission, the exozodiacal dust emission, and residual light from the finite size of the star and a floor to the performance of the stellar suppression. The contribution from the exozodiacal emission is slightly different since, for the IR case, the integrated light from the exozodiacal cloud is seen by each element of the interferometer. This effect results in the interferometer's sensitivity to exozodiacal dust being dependent on the element aperture size (D) and the distance to the star, which affects the exozodiacial dust brightness relative to the local zodiacal dust contribution. The resulting time for detection is

$$t_{IR} = \frac{4}{\pi \Delta \lambda F_0} 10^{0.4\left(2 \cdot m_p\right)} \frac{SNR^2}{D^4 T} \left[10^{-0.4 \cdot z} \pi \lambda^2 206265^2 + \mu 10^{-0.4 \cdot ez} D^2 + \left[\left(\zeta + \frac{\pi^2}{16} \frac{s^2}{\left(\lambda / b\right)^2} \right) D^2 10^{-0.4 m_s} \cdot 4 \right] \right]$$

The first term in the bracket is from local zodiacal dust, the second term from exozody emission (where *ez* is the exozodiacal flux in magnitudes at N band), and the third term is the null leakage from the instrument (ζ) and the star's angular diameter, where *s* is the size of the stellar disc in radians. This calculation assumes the interferometer is a four element design with a nulling baseline of *b* meters. Instrumental parameters in Table 5-1 are from Lay et al. (2007). The light is combined using two successive stages of beamcombiners, so that the zodiacal and planet light is assumed to be split evenly among four interferometric outputs.

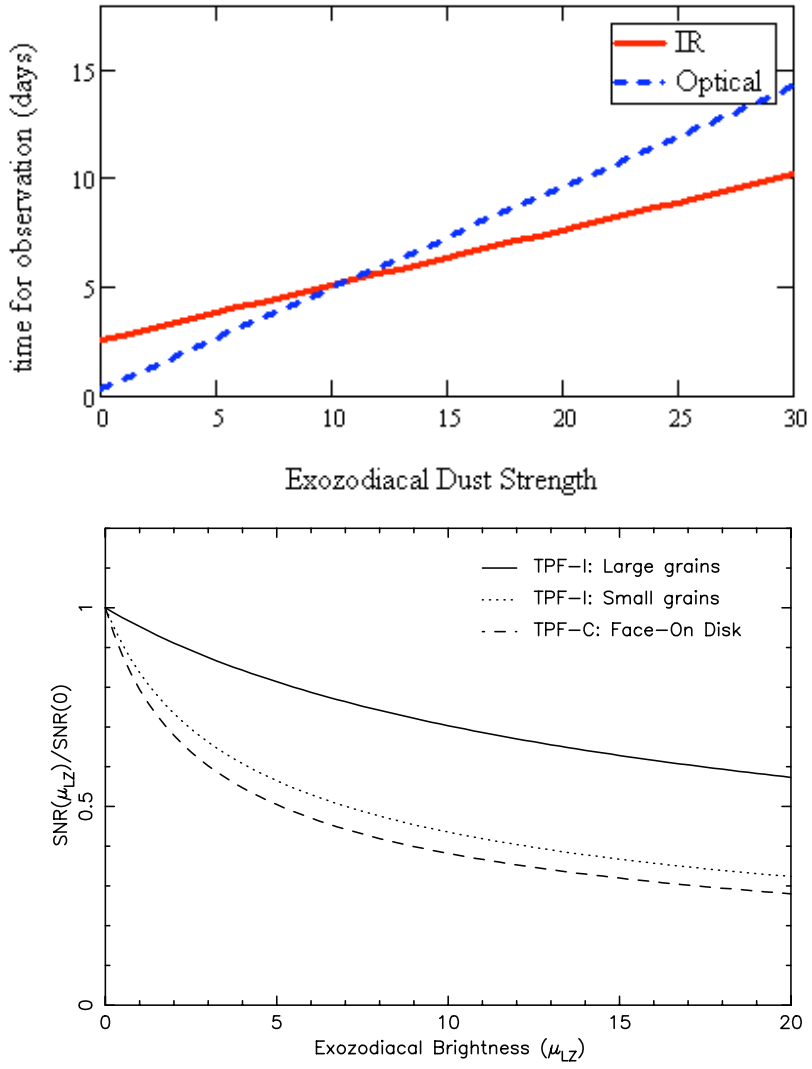

Figure 5-2. Two estimates of the effect of exozodiacal dust on the detection of Earth-like exoplanets. The upper plot shows the effect of exozodiacal dust strength on observing time, based on the equations in the text and using values from Table 5-1. The lower plot shows the estimate of SNR degradation calculated by Beichman et al. (2006).

The time estimates for both cases are necessarily simplistic, not including terms or factors that may refine the actual time needed for a single observation. In this sense the equations may be only approximations of the true time needed. Similarly the values in Table 5-1 are debatable, and can significantly change the resulting plot in Figure 5-2. ***The salient point of the calculations is that exozodiacal emission has the ability to significantly increase the time required for a given observation. This has the cascading effect of reducing the sample size for a mission of a fixed duration.*** This effect can be countered, to some extent by using larger apertures or planning for a longer duration mission. However, it is clear that knowledge of average exozodiacal dust strength is a key input for a robust direct-imaging design reference mission, and indeed knowledge of the exozodiacal levels for all candidate TPF or Darwin stars will allow for a greatly optimized mission and characterization strategy (see Wallner et al. 2008).

5.2 Current State of the Field

The next few years will yield significant progress on the abundance, composition, and morphology of exozodiacal material around nearby stars. Using photometry, spectroscopy, direct imaging, and interferometric observations, the formation and evolution of debris disks, their relationship to planetary systems, and their detectability will be explored.

5.2.1 Photometry

Disks are typically first detected by observation of infrared- to millimeter-wavelength emission in excess of that expected from the central star. This emission is produced when circumstellar dust absorbs emission from the star and re-emits it at longer wavelengths. Models of the dust emission may be fit to the spectral energy distribution (SED) of the system, providing an estimate of the fractional infrared luminosity (L_{IR}/L_{*}) and the effective dust temperature, the combination of which can yield the dust mass.

The most important current mission for the detection and characterization of infrared excesses around solar-like stars is the *Spitzer* Space Telescope. *Spitzer* is capable of making sensitive measurements of exozodiacal clouds at wavelengths of 24 μm, 70 μm, and 160 μm, spanning typical temperature ranges of 40–200 K and corresponding to distance scales of a few to a few hundred AU from the parent star. The sensitivity to exozodiacal emission is limited by *Spitzer*'s photometric accuracy of a few percent at 24 μm and 7–15% at 70 and 160 μm, allowing *Spitzer* to detect or set limits on excesses that are greater than 10–50% above the stellar photosphere.

At 24 μm, this limit corresponds to a factor of 100 to 500 times the level of dust emission in our own Solar System in the distance range of 1 to 10 AU, where 100–200 K dust is located for a solar-type star (see Figure 5-3). At longer wavelengths, the photosphere is weaker, and the corresponding limit is 30–100 times the level of dust in our Solar System between 10–100 AU (~50 K dust). *Spitzer* has already observed or has awarded time for observations of over 200 likely Terrestrial Planet Finder (TPF) target stars (Beichman et al. 2006).

Herschel will be able to search for dust at even cooler temperatures than *Spitzer* with the Photodetector Array Camera and Spectrometer (PACS) instrument. The larger aperture will allow detection of dust at lower optical depths for the outer regions of planetary systems. The expected sensitivity level is equivalent to an optical depth of approximately 10^{-6} for very cold dust (see Figure 5-3).

5.2.2 Disk Imaging

Spectral Energy Distribution (SED) fitting can provide some information on the existence and spatial distribution of the dust (for example, the presence of central holes in the dust disk), but, due to contribution from the star, photometric detection, starting at wavelengths shorter than approximately 30 μm, is increasingly difficult for faint levels of dust emission. Imaging of the disk provides two advantages over photometry: separation of unresolved (starlight) and resolved (disk) emission, and determination of the morphology of the debris disk. In principle, imaging should provide fainter levels of detection, compared to photometric limits, particularly for warm dust, within the habitable zone around a star. In addition, large planetary bodies can create asymmetries in the disk structures that would go unnoticed with photometry alone.

Spitzer

Spitzer has been able to image the thermal emission from dust in debris disks around the closest stars such as Fomalhaut and Vega. The thermal and scattering properties of the disks allow us to place constraints on the amount and size of the dust grains in the disks. But, perhaps more importantly, the presence of asymmetries within the disks may indicate the presence of large planetary bodies orbiting the host stars. For example, in the *Spitzer* images of Fomalhaut (Stapelfeldt et al. 2004), the disk is asymmetric at both 24 and 70 μm, and in the *HST* image (Kalas et al. 2006), the disk is found to be off-center from the position of the star. An unseen planet may have given rise to these asymmetries.

Nulling Interferometry

Information on dust in the inner regions of disks will come from two ground-based nulling interferometers planned to come into operation over the next few years: the Keck Interferometer and the LBTI. Keck Interferometer observations are currently capable of detecting exozodiacal disks with a 1-σ noise limit, which corresponds to approximately 100 zodis. The LBTI, planned for operation beginning in 2010, has a significantly different architecture than KI, which greatly reduces the thermal background and stellar suppression, enabling detection of much fainter disks. LBTI is designed to reach a 3-σ limit of 10 zodies for a sample of nearby stars (see section 5.3.2 for expected performance). These observations will help determine whether many or all stars have more than 10 times the level of zodiacal dust in our Solar System, which would likely be a complication for efforts to image terrestrial planets in the habitable zones of nearby stars.

Scattered Light Imaging

HST observations of dust disks in scattered light have provided interesting insights into many nearby systems. Detection of disks such as those around Fomalhaut (Kalas et al. 2006) and β Pictoris (Golimowski et al. 2006), has demonstrated the ability to detect material with optical depths of 10^{-4}–10^{-3} (1000–10000× the solar zodiacal level), on scales of 10–1000 AU. The inclination of β Pic's inner disk (Heap et al. 2000) is consistent with a planet sustaining this structure. These observations are typically sensitive to dust in regions comparable to the Sun's Kuiper belt.

In scattered light, about four dozen primordial (protoplanetary) disks have been resolved, plus a similar number of disks seen as silhouettes against bright nebulosity in Orion (so-called proplyds). The census of debris disks resolved in scattered light is much smaller, less than 20 objects. An up-to-date catalog of all these resolved objects may be obtained from

http://circumstellardisks.org. The optical depths of these resolved disks range from a high of 3 × 10^{-3} (e.g., Beta Pic, HD 181327) down to about 10^{-4} (e.g., Fomalhaut, HD 139664). The majority of such disks have been imaged using the *Hubble Space Telescope* (e.g., Grady et al. 1999; Schneider et al. 1999; Clampin et al. 2003; Krist et al. 2005). Adaptive optics imaging has shown increasing promise in recent years, particularly through reducing the residual speckle pattern through either angular differential imaging (e.g., Fitzgerald et al. 2007; Kalas et al. 2007) or simultaneous polarimetry (e.g., Apai et al. 2004; Perrin et al. 2004).

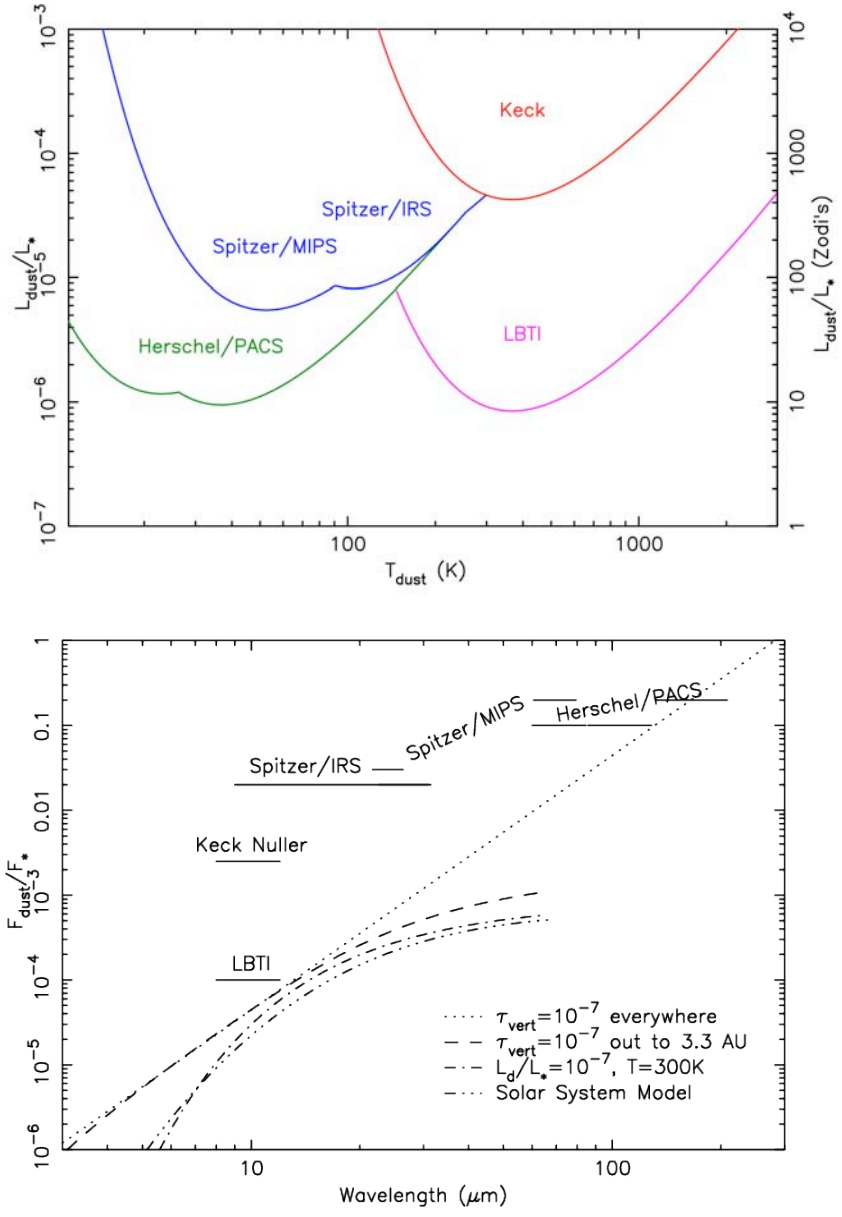

Figure 5-3: Sensitivity limits for detection of dust around nearby solar-type stars. The two plots show the limits in terms of temperature of the dust (top) and detection wavelength (bottom). 3-σ detection limits are shown in terms of the dust's fractional luminosity (L_{dust}/L_*, left) or fractional flux (F_{dust}/F_*, right). The assumed 1-σ accuracies are 20% of the stellar flux for *Spitzer*/MIPS at 70 μm, 2.5% for *Spitzer*/IRS at 32 μm, S/N = 10 for Herschel/PACS at 100 μm, S/N = 2 for Herschel/PACS at 160 μm, 0.5% null for Keck Interferometer at 10 μm, and starlight removal to 0.01% for LBTI at 10 μm. (G. Bryden, JPL)

Though not specifically designed for high-contrast imaging, *HST* is extremely stable, allowing for significant reduction of the stellar point-spread function by subtracting a reference image of another star or the same star observed at a different orientation. *HST* has three coronagraphs: in the NICMOS camera (0.9–2.2 μm, multiple filters), in the STIS spectrograph (0.2–1.1 μm, unfiltered), and in the ACS HRC camera (0.2–1.1 μm, multiple filters). None of these are optimized, however, and with no wavefront-control mechanisms, the bulk of the contrast gain is achieved through PSF subtraction. ACS and NICMOS have complementary strengths in this area, with ACS offering better overall scattered light rejection, hence greater sensitivity, while NICMOS has a smaller inner working angle. At the moment the STIS and ACS cameras are nonoperational, though they are expected to be repaired during the *HST* servicing mission scheduled for near the end of 2008.

Observations in scattered light have allowed us to move beyond an initial reconnaissance of disks towards the detailed characterization of their compositions and three-dimensional structures. Multiwavelength and polarimetric imaging have provided significant insights into the detailed properties of the dust grains that comprise these disks, and thus given us better understanding of the physical processes, which act upon grains. Because different wavelengths are most sensitive to particles of different sizes, broad wavelength coverage is essential to fully assess the overall dust distributions (e.g., Metchev et al. 2004; Fitzgerald et al. 2007; Pinte et al. 2007).

Polarization of light is a fundamental aspect of the scattering process, depending on the properties of the scattering particles and the scattering geometry, and thus polarization is an indispensible diagnostic of grain properties. This is particularly true for edge-on disks, where polarization breaks the degeneracy between dust properties and the radial distribution of dust. In an edge-on disk, without polarization we cannot tell the difference between a disk with constant density and strong forward scattering and a disk with a steep radial density gradient and isotropic scattering. Measurement of linear polarization breaks this degeneracy and allows unambiguous measurement of grain properties such as porosity (Graham et al. 2007). Polarimetric studies of dust grain properties remain currently underway with NICMOS on *HST*, and will hopefully return with a revitalized ACS in the future as well.

We emphasize that together the combination of visible and near-infrared imaging (and mid-infrared, when available) provides significantly greater insight into dust properties than any single wavelength alone. Krist et al. (2007) suggest that *JWST* will be no better than *HST* at the shorter wavelengths (1–2 μm) for imaging debris disks; however, Doyon et al. (2008) have shown that spectral differential coronagaphy using *JWST*'s Tunable Filter Imager will deliver better performance. *JWST* also offers new coronagraphic capabilities with high-performance coronagraphic imaging from 2.5–28 μm (Clampin et al. 2007). *JWST* will offer significant opportunities for imaging the present sample in the mid-infrared where a rich selection of spectral diagnostics of grain properties are available. Over the last few years, new debris disks have been resolved at a rate of 2–4 per year, and the planned repair of ACS this fall is a high priority to enable this trend to continue. The currently resolved disks represent just the tip of the iceberg. Less than a quarter of the debris disks detected by IRAS have since been resolved in scattered light (cf. Figure 5-4), to say nothing of the much larger sample of debris disks detected by *Spitzer*. However, the greatest progress in this area will require several orders of magnitude increased contrast compared with present systems. Two orders of magnitude improvement in contrast would allow the entire set of IRAS-detected disks to be imaged in scattered light (though still leaving us unable to image disks less than 100× the solar zodiacal level). Since disks broadly trend to lower optical depths at

greater ages, an increased sample size of resolved disks would allow studies across a broader range of ages and evolutionary states than now available.

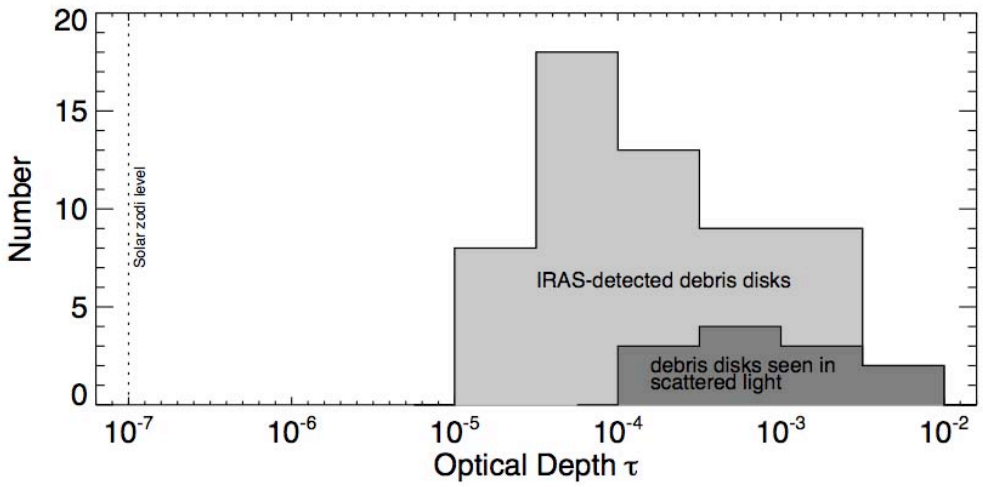

Figure 5-4: Debris Disks detected from thermal emission and scattered light. Currently, only a small fraction of the known debris disks in the Solar neighborhood have been resolved in scattered light. This figure shows histograms of the known nearby debris disks detected by IRAS (from Zuckerman & Song 2004), compared with a histogram of the debris disks which have been resolved in scattered light (data from Paul Kalas and circumstellardisks.org). (M. Perrin, UCLA)

In the near term, new high-contrast adaptive optics systems hope to provide at least an order of magnitude contrast over present capabilities. The Gemini Planet Imager (GPI), currently under development for first light at Gemini in early 2011, has a science requirement to image disks down to an optical depth of 3×10^{-5}, for target stars of I < 8 mag. GPI will attain this goal using its high-order adaptive optics system with a dual-channel infrared imaging polarimeter that uses a lenslet array to pixellate the image plane prior to polarization beam-splitting, thereby minimizing non-common path errors. Similarly ESO's SPHERE high-contrast AO system will include both near-infrared and visible light dual-channel polarimetry, with comparable contrast goals. The characteristic inner working angles of these systems will be ~0.2 arcsec, and their contrast will decrease outside of the ~1"-wide dark hole created by the AO system. Hence for typical target distances of 20–100 pc, they will be most sensitive to dust on scales of 5–100 AU, comparable in scale to the outer Solar System and Kuiper belt. Dust in or near the habitable zone will remain inaccessible to these systems except for the closest targets.

NIR Interferometery

Although most debris disks do not show a clear near-infrared excess in their spectral energy distributions, limits set by spatially unresolved broadband photometry are generally not better than a few to several percent. A small, warm dust component could be present if dust generated by collisions migrated close to the star or was produced by bodies in close orbits. If located within a few AU of the central star, this dust would be at temperatures that would produce near-infrared emission, and small grains would produce scattered light. Detection of (or stringent limits on) warm dust will characterize the inner portions of these debris disks. The spatial resolution of infrared interferometry can be exploited to probe for warm dust in these systems. On long baselines (> 100 m) the central star is resolved, and the visibility is primarily a measure of the stellar photospheric size. On shorter baselines

(< 50 m) the photosphere is mostly unresolved, and if the measured visibilities have high accuracy, one can search for emission by looking for deviations from the visibility expected for the stellar photosphere. Any resolved or incoherent emission will decrease the measured visibility from the stellar value.

Obtaining sufficient observational precision currently limits such studies of near-IR excess to the closest and brightest debris systems, and to date, most observations have been of A star systems. Detections have been made of 1–2% near-infrared excesses for the A stars Vega (Ciardi et al. 2001; Absil et al. 2006), ζ Aql (Absil et al. 2008) and β Leo (Akeson et al. 2009) and only 1 lower mass star, τ Ceti (di Folco et al. 2007). To be consistent with both the near-infrared excess and the previously known mid- to far-infrared excess requires a ring of small, hot dust near the sublimation radius. Given the small number of objects observed so far, it is not clear if these inner hot dust rings are due to transient events or are the product of collisions between larger bodies orbiting close to the star. We discuss the performance of current and near future interferometers in more detail in section 5.3 below.

5.2.3 Spectroscopy of Dust and Gas

Information on the nature (e.g., size and composition) of the dust grains in debris disks is vitally important to our understanding of planetary system formation and evolution. In particular, the composition of the dust grains is likely directly related to the composition of any unseen planetary bodies. For example, *Spitzer* spectroscopic observations of HD 69830 reveal a rich spectrum of silicates and carbonates similar to that seen on certain classes of asteroids in the Solar System (Beichman et al. 2005; Lisse et al. 2007). The observed dust may be the result of asteroids colliding in a massive belt, producing copious amounts of small grains in the habitable zone around HD 69830.

Interestingly, HD 69830 shows no infrared excess at longer wavelengths (70 μm), indicating that the presence or extent of a debris disk around potential TPF targets cannot be determined unambiguously from single wavelength observations. A *Spitzer* spectroscopic survey for warm dust around TPF target stars finds only a few stars with silicate emission, for an overall detection rate of just ~1% (Beichman et al. 2006).

Spectroscopy of circumstellar gases may provide information on the composition of the disk and its constituent bodies that is less readily available from dust observations. In addition, the gas abundance in debris disks is important for modeling of dust structures that have been attributed to the gravitational influence of unseen young planets (e.g., cleared zones, dust rings, and clumps).

Detections of gas in debris disks have been achieved with optical and ultraviolet spectroscopy. Except for one case, observation of resonantly scattered gas emission from β Pic at optical wavelengths (Olofsson et al. 2001; Brandeker et al. 2004), these detections have always involved absorption spectroscopy of edge-on disks. Such observations are sensitive to very small amounts of cold gas. Unfortunately, the geometric constraint that the line of sight to the central star must pass through the disk severely limits the number of disks that may be probed for gas in this way. In the longer-term, an ideal instrument to detect gas in debris disks and also to image new disks uncovered by *Spitzer* will be the Atacama Large Millimeter Array (ALMA), which is expected to begin operation late in this decade. With 64 antennas of 12-m aperture spread across baselines extending to 10 km, ALMA will achieve a spatial resolution of 30 mas (0.5 AU at β Pictoris; 4 AU in nearby star-forming regions). ALMA will provide detailed maps of the density, kinematic structure, and chemical structure of protoplanetary disks in molecular and atomic line emission, and of the

dust continuum emission of nearby debris disks. With no stellar contrast problem at these wavelengths, ALMA should map more disks in greater detail than any prior astronomical facility.

5.2.4 Theory and Modeling

Observations of debris disks often reveal structures (such as rings, clumps, and warps) that are generally attributed to the gravitational influence of unseen planets (e.g., Heap et al. 2000; Holland et al. 2003). Analogous structures in our Solar System are the very narrow rings within Saturn's ring system confined by shepherding satellites and the apparent circumsolar resonant ring structure created by Earth (Dermott et al. 1994). Recognizing these structures in images of exozodiacal clouds and debris disks can allow us to indirectly detect exoplanets and measure their masses and orbital parameters. Observations of such structures may be the only way to detect Neptune- and Earth-mass planets located beyond ~10 AU from their host stars, where orbital periods are too long for radial-velocity, transit and astrometric techniques, and where these planets are too faint to detect directly in reflected starlight or thermal emission. In addition, unresolved clumps in an exozodiacal dust disk might initially be mistaken for a terrestrial planet.

Modeling Observed Debris Disks and the Origins of Planetesimal Belts

The most well studied debris disk is that of our own Solar System, which exhibits the zodiacal cloud of dust due to collisions between asteroids and the outgassing of comets, and the Kuiper belt of small icy bodies. The orbital distribution of Kuiper Belt Objects (KBOs) in the outer Solar System suggests that a large fraction of planetesimals are scattered outward as a consequence of gravitational perturbation by giant planets, and a significant fraction of KBOs are trapped in mean motion resonances with Neptune. These observations, among others, imply that the Kuiper Belt and the outer planets of our Solar System are historically linked. A recent breakthrough in theoretical modeling has produced the first model, known as the Nice Model, which simultaneously explains these features and the orbital distribution of the giant planets, the Trojans of Jupiter and Neptune, and the Late Heavy Bombardment (Tsiganis et al. 2005; Morbidelli et al. 2005; Gomes et al. 2005). The Nice Model reproduces all of these signatures by modeling the outward migration of the giant planets in a planetesimal disk truncated at the current location of Neptune. The Nice Model demonstrates the importance of planetary migration models and gives credence to future models that will attempt to describe the origin and distribution of the residual planetesimals in debris disks.

Models of planetary migration have already been applied to extrasolar debris disks with some success. In currently-observed debris disks that exhibit optical depths greater than ~100–1000 zodis, collisions dominate the dynamics. Due to the dust grains' short collisional lifetimes, some modelers have interpreted the observed ring structures as tracers of the sources of dust. Models of such disks have focused on capturing planetesimals, the parent bodies of dust particles, into resonances via planet migration (Wyatt 2003; Reche et al. 2008). Simulations that have investigated capture probabilities of planetesimals as a function of planet migration parameters have suggested that we may be able to learn about the migration history of a system from the appearance of a ring structure (Wyatt 2003). Similar migration models have also shown that the eccentricity of the planet's orbit and initial eccentricity of the planetesimals' orbits must be very low

(< 0.1) for the resulting ring structure to exhibit any azimuthal asymmetry (Reche et al. 2008).

Other models of collisionally dominated disks have focused on the size distribution of dust in collisional equilibrium and the outcome of transient collisional avalanche events (Krivov et al. 2007; Grigorieva et al. 2007). We have learned that while collisional avalanches can lead to brightness asymmetries in an edge-on disk similar to those that may exist due to resonant trapping of dust particles, the probability of witnessing an avalanche event is on the order of a few percent for a disk with as much dust as Beta Pic (Grigorieva et al. 2007).

Several observed collisionally dominated disks harbor dynamically significant quantities of gas. Takeuchi & Artymowicz (2001) showed that a relatively modest amount of gas will strongly affect the dynamics of small dust grains, which are the grains most easily seen in optical and near- to mid-infrared disk images, and this can lead to the formation of azimuthally symmetric structures, such as cleared zones or dust rings, without the gravitational influence of a planet. This general conclusion is supported by more recent modeling (Klahr & Lin 2006), which also showed that such gas-formed structures can persist after the gas is completely gone. These effects may be a significant source of confusion for young transitional debris disks.

Predictions for Exozodiacal Disks

Other than results from the Keck Interferometer or LBTI, most observations of dust prior to TPF-C and TPF-I will not measure dust emission originating from the habitable zone. In the absence of these measurements, we may be tempted to use observations of dust at larger circumstellar distances to estimate the dust abundance in the habitable zone. However, extrapolating an observed abundance of dust from large circumstellar distances inward to the habitable zone of a given system is a precarious task. Unknown sources and sinks of dust may exist in these systems interior to the regions where these missions will observe. For example, our Solar System has many sources of dust interior to the Kuiper belt: comets, main belt asteroids, Trojan asteroids, etc. Exoplanet discoveries have revealed a surprising variety of planetary systems, and we have no reason to believe that the diversity of dust producing bodies will be any less surprising. Understanding the dust in the habitable zones of nearby stars will probably require both observations directly sensitive to habitable-zone dust, and also modeling efforts to interpret these observations.

With future observatories, we expect to directly image exozodiacal disks analogous to our own zodiacal cloud, with optical depths on the order of $\sim 10^{-7}$. Long-term dynamical effects, such as migration due to Poynting-Robertson and corpuscular drag, are important in these tenuous disks. Models have largely ignored collisions altogether and focused on dust-capture into a planet's exterior mean motion resonances as the dust migrates inward under the influence of drag (e.g., Jackson & Zook 1989; Dermott et al. 1994; Liou & Zook 1999; Moro-Martín & Malhotra 2002; Wyatt 2006).

Models of these steady-state zodiacal cloud structures have come a long way since Dermott et al. (1994) first recognized the leading/trailing asymmetry in the surface brightness of the infrared sky as a circumsolar ring of zodiacal dust trapped in resonance with the Earth. We now more-or-less understand the geometry of resonant signatures from analytical calculations (Kuchner & Holman 2003) and numerical simulations (e.g., Moro-Martín & Malhotra 2002; Deller & Maddison 2005). Figure 5-5 qualitatively illustrates the basic geometries of resonant structures created by a single planet in a collisionless dust cloud (Kuchner & Holman 2003). Basic numerical models have also revealed that planets on

eccentric orbits can trap particles in resonant terms that produce density structures which appear to revolve at mean rates slower than the mean motion of the perturbing planet (Wilner et al. 2002).

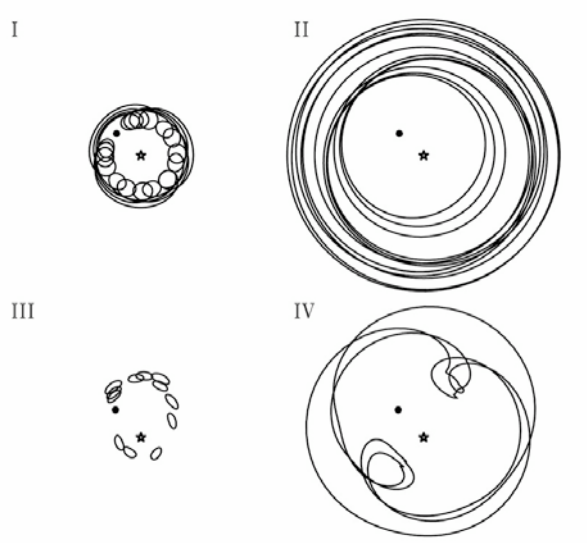

Figure 5-5. Approximate analytic description of the range of resonant structures a single planet can create in a collisionless cloud. Case I, a ring with a co-rotating gap at the location of the planet is exemplified by Earth's interaction with the solar zodiacal cloud. The other cases have been suggested as models for other debris disks, but not yet verified. (Kuchner & Holman 2003)

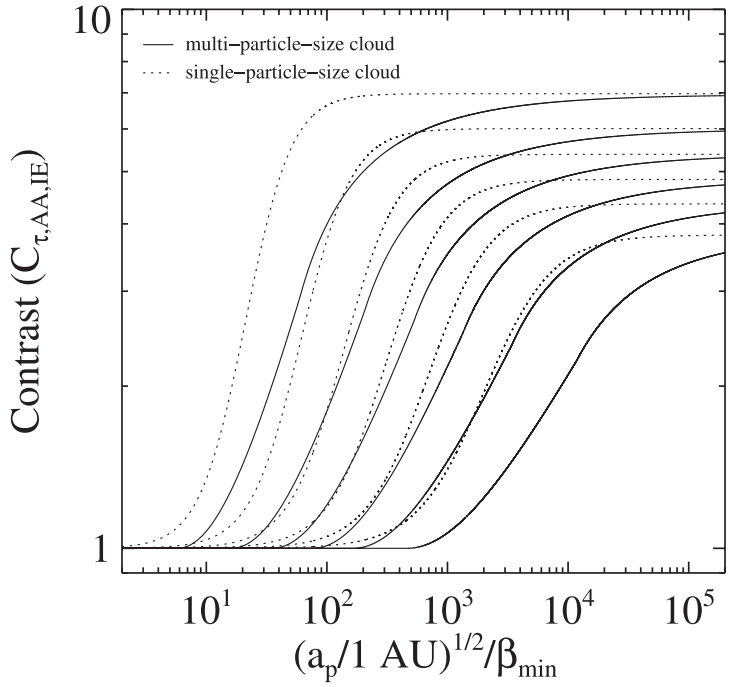

Figure 5-6. Contrast in optical depth for multi-particle-size clouds (solid lines) assuming a Dohnanyi (1969) crushing law compared to single-particle-size clouds (dashed lines). From top to bottom, the six solid lines and six dashed lines correspond to six values of planet mass: 5, 2, 1, 0.25, and 0.1 $M_{\oplus}$. The contributions of the small grains reduce the contrasts of the multi-particle-size clouds compared to single-particle-size clouds with the same minimum value of β, where β is the ratio of the force due to radiation pressure to the gravitational force on a dust grain and is proportional to s^{-1}, the radius of the dust grain. (Stark & Kuchner 2008)

Recent advances in collisionless disk models have allowed for a number of quantitative predictions regarding the morphology and contrast of resonant structures formed by terrestrial-mass planets. These models have shown that most resonant structures feature a sharp inner-edge at a circumstellar distance of 83% of the semi-major axis of the planet, a gap in the ring structure at the location of the planet, which varies in size linearly with ring brightness (from a few degrees to nearly ninety degrees), and ring widths that vary from a few percent to 1.6 times the semi-major axis of the planet. The same models have shown that a degeneracy exists in particle size, s, and planet semi-major axis, a_p; two exozodiacal ring structures can be geometrically identical for a constant value of ($sa_p^{1/2}$) (Stark & Kuchner 2008).

Models of collisionless exozodiacal clouds of a single grain size estimate that the contrast, defined as the ratio of optical depth within the ring structure to outside of the ring structure, of resonant ring structures created by terrestrial-mass planets can vary from unity to 7:1, as shown in Figure 5-6. This figure also illustrates that a distribution of particle sizes tends to wash out ring structures, reducing their contrast by up to ~50% (Stark & Kuchner 2008). Figure 5-7 shows the minimum detectable planet mass that can be indirectly detected via observations of its resonant ring structure, assuming a distribution of particle sizes and a minimum detectable ring contrast of 1.5:1. These estimates assume the dust is produced entirely by a source analogous to our asteroid belt; no highly-inclined or highly-eccentric sources contribute to the production of dust, and thus Figure 5-7 can be thought of as a best-case scenario.

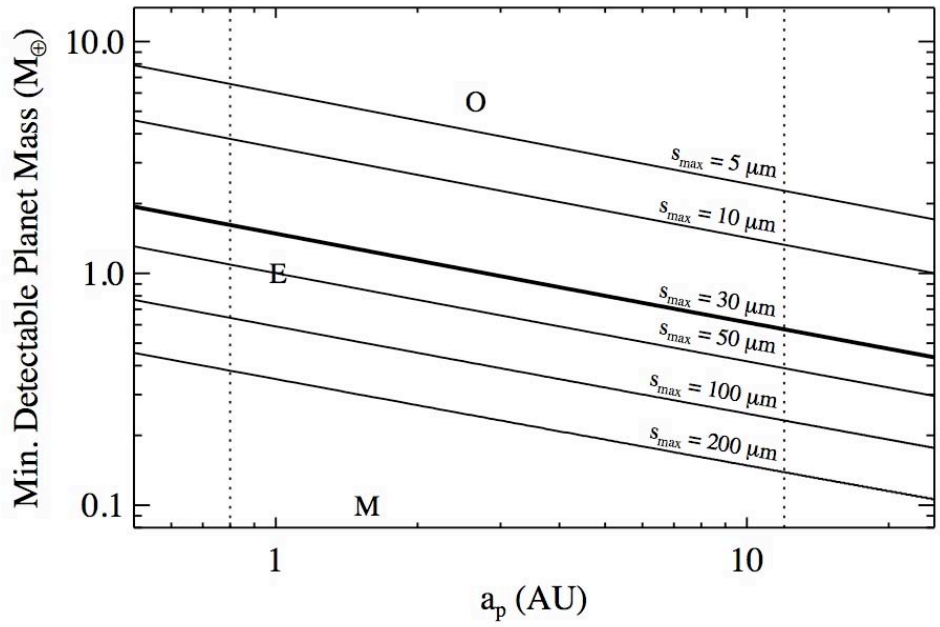

Figure 5-7. Minimum detectable planet mass in a multi-particle-size collisionless cloud as a function of semi-major axis, a_p, and maximum grain size, s_{max}, assuming a Sun-like star, a minimum detectable ring contrast of 1.5:1, and dust produced according to a Dohnanyi (1969) crushing law. Earth-like and Mars-like planets are denoted with an *E* and *M*, respectively. The 5.5 $M_\oplus$ exoplanet OGLE-2005-BLG-390Lb is denoted with an *O*. Listed values for maximum dust size in the ring structure assume perfectly absorbing spherical grains with mean density ρ = 2.0 gm cm^{-3}. The bold line shows the case of the solar zodiacal cloud, for which the observed emission is dominated by 30-μm grains. The dashed lines show typical inner and outer detection limits for a mission similar to TPF. (Stark & Kuchner 2008)

5.3 Technology Development and Performance Demonstration

The technology development section focuses on the development of nulling interferometry in particular as the key technology needed to advance our knowledge of dust in the habitable zones around nearby stars. This technique has been developed for the Keck Interferometer and the Large Binocular Telescope Interferometer (LBTI), with prototype testing for LBTI being carried out on the Multiple Mirror Telescope (MMT).

5.3.1 Past Accomplishments

Interferometric nulling of thermal emission from stars was demonstrated for the first time in 1998 using the MMT. By interfering infrared radiation from two of the co-mounted 1.8 m telescopes, the stellar image was suppressed by a factor of order 25 and used to map directly the thermal emission of warm dust surrounding Betelgeuse (Hinz et al. 1998).

The MMT was rebuilt as a single 6.5-m telescope early in the decade and outfitted with an adaptive secondary mirror in 2002. To facilitate testing in preparation for LBTI, a cryogenic nulling interferometer called the Bracewell Infrared Nulling Cryostat (BLINC), was developed (Hinz et al. 2000). The instrument creates a pseudo-interferometer with elliptical 2.5 × 5-m apertures across a 4-m baseline. Phase variations between the beams are sensed using 2.2-μm light that travels an identical path to the light at 11 μm. A dispersion introduced into the system creates a null, that is both achromatic across the science band and creates a suitable phasing signal at 2.2 μm (see Hinz et al. 2000 for more information). The instrument is mated with a Mid-Infrared Array Camera (MIRAC) that measures the amount of flux in the nulled output of the BLINC.

Nulling interferometric techniques have been developed at JPL and are described in detail in Chapter 4. These techniques have been adapted for use in the KI nuller and are now in regular use at the Keck Interferometer.

The Keck Interferometer combines the two 10-m Keck telescopes as a long baseline interferometer, funded by NASA, as a joint development among the Jet Propulsion Laboratory, the W. M. Keck Observatory, and the NASA Exoplanet Science Institute. The KI nuller (Serabyn et al. 2004; Colavita et al. 2006, 2008) is implemented as a four-beam system operating at a wavelength of 10 μm. The two Keck telescope apertures are split into left ("primary") and right ("secondary") halves at a dual-star module (DSM) at each telescope. Accounting for diffraction and other details, the beam size on the sky at 10 μm is approximately 0.45'' × 0.50''. Two modified Mach-Zehnder beamsplitters combine the light from the left halves and right halves on the long 85-m baseline. The outputs of the two long baselines are combined in a beamsplitter—the cross combiner—with a short 4-m effective baseline. The output of the cross combiner feeds a mid-IR camera, KALI. Modulation on the long baselines is used to chop the central star to detect surrounding extended emission, while modulation on short baseline allows fringe detection in the presence of the strong thermal background. Because of the limited measurement and control bandwidths achievable in the integration times required to observe faint 10-μm sources, phasing and tilt stabilization rely upon feed-forward from two 2-μm fringe trackers (i.e., phase-referencing, or cophasing), as well as tilt feed-forward from the KI angle tracker operating at 1.2 or 1.6 μm. Laser metrology and accelerometer feed-forward is used to stabilize against non-atmospheric disturbances. A distributed real-time control system controls the various

servos and interconnections, aided by high-level sequencers. See Colavita et al. (2008) for more details.

5.3.2 Performance

Keck Interferometer is currently operational and is performing Key Science surveys. The LBTI is being completed with operation anticipated for 2010. The performance, demonstrated and expected for each facility, is described below.

Keck Interferometer

The current observational approach for the Keck Interferometer is to divide the night into three segments, each one dedicated to a single science target. Accounting for overheads, this is well matched to the ±14-m usable contiguous delay range for the nuller delay lines; this range allows for 2–3 hour delay tracks on the science targets. The observations goal is for two or three science scans with interleaved, bracketing calibrators with between 10 and 15 minutes of null/peak data on each target, depending on the source brightness. Including more than one calibrated scan per cluster allows for better estimates of the external errors, rather than relying on formal errors from the internal scatter of a single observation. Repeated observations on subsequent nights provide confidence in the nightly external errors.

A series of performance-validation tests were performed between June and Aug. 2007, which revealed a slight, but statistically significant, night-to-night bias. This was ultimately traced to an additive long-wavelength leakage term whose impact was flux dependent. The most likely explanation for the bias appears to be radiation from structure at the telescope top end that is diffracting into the beam path and introducing correlated emission into the two halves of each aperture. By changing the adaptive optics rotator offset angle, which changes the orientation of the pupil split on the telescope, and thus the geometry of top-end structure with respect to the cross-combiner baseline, this long-wavelength leakage could be substantially reduced, although not completely eliminated. Observationally, more carefully matching target and calibrator fluxes reduced the size of the effect, and shifting the broadband null reduction bandpass slightly toward shorter wavelengths also reduced the magnitude of the effect. With these three changes, the biases attributable to this effect have been shown to be much smaller than the external error per cluster based on 21 science clusters measured through April 2008. From analysis of this data set, the KI achieved an external error per cluster computed from the error of the calibrated scans of approximately 0.25% RMS in a broadband 8–9 μm channel. This value is equivalent to 100 zodi RMS (where 1 zodi is the flux produced by the zodiacal dust within our own Solar System) after accounting for transmission through the long-baseline fringe pattern.

NASA has allocated a substantial portion of its 2008 Keck time to Key Science projects with the nuller. Three Key Science teams were selected in Nov. 2007; the PIs of the teams are Phil Hinz, Univ. of Arizona; Marc Kuchner, Goddard Space Flight Center; and Gene Serabyn, JPL. The key science observing program is currently underway, and by the time it completes in Feb 2009, will have observed roughly 40 nearby main-sequence stars, which are potential targets for future planet-finding missions and stars with known debris disks. The continued operation of KI for nulling observations after February 2009 is uncertain; no funding is being planned after this time period.

LBTI

The Large Binocular Telescope Interferometer is a common-mount design interferometer with 8.4-m apertures on a 14.4-m baseline. The common-mount design negates the need for long delay lines. Only three warm mirrors (primary, secondary and Nasmyth flat) are used to direct the beams toward the central instrument platform. This is especially important for thermal infrared (> 3 μm) observations where telescope emissivity can be the dominant source of noise. The deformable elements of the AO systems of the LBT are integrated into the secondary mirrors of the telescope, which form the aperture stop of the telescope to optimize infrared performance. Extra surfaces in a conventional AO system add a significant amount of background light in the thermal infrared, decreasing the system's sensitivity. These several unique aspects of the LBTI allow for efficient high sensitivity beam combination that is well matched to the goals of thermal infrared detection of zodiacal dust.

Very deep stellar suppression can be achieved with nulling interferometry. The fundamental limit to this approach is the angular size of the star compared to the baseline of the interferometer. For a solar type star at 10 pc this limit is below 10^{-4} for the LBTI. At the same time the LBTI will be sensitive to dust $\lambda/2b$ away or approximately 0.7 AU for a star at 10 pc. This combination of deep stellar suppression achievable, low background in the thermal infrared, and good spatial resolution for nearby stars will enable the LBTI to probe nearby stars for zodiacal dust to an unprecedented level.

Performance estimates for the LBTI are based on observational tests being carried out with the Bracewell Infrared Nulling Cryostat (BLINC) on the MMT. Although primarily intended as an engineering prototype, BLINC can probe the very nearest and brightest stars for which the region of emission at 11 μm is comparable to $\lambda/2b$, or 0.25 arcsec. Initial results have been demonstrated by probing for zodiacal dust around Vega (Liu et al. 2004). The 1-σ uncertainty in the null is approximately 7×10^{-3} for observations of Vega, equivalent to an approximately 200-zodi dust disk around Vega. More recent observations (spring 2008) have reduced this uncertainty to approximately 1×10^{-3} within a specific observation sequence, but with a systematic variation which is three times larger.

The level of the null uncertainty at the MMT is expected to be limited primarily by the performance of the adaptive optics correction. For the parameters of the MMT system, a variation in the characteristic scale of atmospheric turbulence, r_0, by 50% over the time of observation will limit the null to approximately 8×10^{-4}, in agreement with the internal error measured at the MMT. The suspected source of the systematic change is variations in telescope vibration under differing wind conditions and azimuth angles of the telescope. More careful calibration and improvements of the telescope pointing should alleviate this affect in future runs, but it remains to be demonstrated that the systematic variations can be kept below the statistical variations introduced by changes in atmospheric seeing.

To properly estimate limits to detection of zodiacal dust with LBTI it is important to understand photometric detection limitations, and null depth and stability limitations. The former limits the detectable dust for later-type stars and stars further away, and the latter limits dust detection around even the closest, early-type stars. At 11.1 μm a telescope emissivity of 7% for the LBT gives a background flux of 1.6×10^{10} photons·s^{-1} for a 20% passband. The sky background from a HITRAN model atmosphere (Gillett & Mountain 1998) is expected to be 3.4×10^{9} photons·s^{-1}. If the total throughput is set at 25%, the 5-σ limit to sensitivity is 100 μJy per $\sqrt{hour}$ of integration for the LBTI. This photometric uncertainty is sufficient to detect dust disks 0.5, 2, 9, and 100 times solar for a F0, G0, K0,

and M0 star at 10 pc, respectively. As discussed above, the detection of dust is weighted toward earlier type stars.

For good photometric sensitivity, detection limits are set in practice by the level of null uncertainty. For the AO performance of the LBT, the null uncertainty in a typical observation is expected to be approximately 1.2×10^{-4}. This is nearly six times better than the MMT and is due to two effects: the larger apertures of the LBT, relative to the MMT, and the faster update rate of the LBT AO system (1 kHz, versus 500 Hz for the MMT). This null uncertainty is equivalent to approximately a dust disk that is 3 times solar. At this level confirmation of detection of a signal will be obtained by comparing spectral information of the residual flux. Flux from a dust disk will be reasonably constant in flux across the the 8–13 μm passband, while residuals from poorly suppressed starlight will follow a Rayleigh-Jeans $1/\lambda^2$ spectral slope.

5.3.3 Future Developments and Milestones

Future effort in studying exozodiacal disks will focus on increased sensitivity observations with the LBTI and Herschel, developing improved modeling and theoretical predictions of dust disk-planet interactions, studying the use of ELTs for exozodical detection, and exploring concepts for an exozodiacal precursor mission.

LBTI Milestones

The Large Binocular Telescope saw first light with the first primary in October 2005. The telescope is currently in use for astronomical observations using prime-focus wide-field imagers. For interferometric operations adaptive secondaries are required. These are planned for delivery in March 2009 and November 2009 for the first and second secondary, respectively.

The LBT Interferometer is currently being assembled and tested at Steward Observatory. In summer 2008 it was shipped to the LBT on Mt. Graham for initial integration with the telescope. Ongoing tests are planned as the adaptive secondaries are completed. Once the adaptive secondaries are integrated with the telescope, approximately one year of testing and commissioning observations will be required prior to routine exozodiacal observations. On the current schedule this would result in scientific operations beginning in late 2010 to early 2011. Future operation of the LBTI is still in question, because NASA funding plans currently only cover the completion of the instrument.

The LBTI is being developed specifically to carry out a Nulling Infra-Red Extrasolar Survey for TPF (NIREST, as in the "nearest" stars). This will involve observations of a comprehensive sample (60–80) of nearby, main-sequence stars. In addition to characterizing candidate systems for TPF, the survey will provide useful insights into the prevalence of exozodiacal dust with various stellar parameters.

The sample, as currently composed, has approximately 15 stars in each spectral type bin A, F, G, and K, with 8 M spectral type stars. Age determination will be an additional factor that will factor into our final source selection. Each star is anticipated to require 4 hours to achieve a reasonable signal to noise level. The total survey will then require on the order of 40–60 nights. A sample with approximately equal number of stars in three age bins of 0–1, 1–2, and 2–3 Gyr, will be constructed to allow a rough determination of zodiacal dust with both spectral type and age of a star.

Theory Development

There is much more numerical and analytical work to be done to provide a sound framework to understand the possible range of long-lived structures that may persist in an exozodiacal cloud. Future models must focus on disks for which both collisions and long-term dynamical evolution are important. Understanding collisional effects is crucial to understanding the dynamics of most currently known debris disks, which have optical depths 100–10,000 times that of the solar zodiacal cloud. The number of observed collisional disks is expected to grow significantly in the next few years with the observations of *JWST*, Keck, ALMA, and LBTI. Interpreting these images hinges on improved models of collisional dust clouds (e.g., Wyatt 2005; Krivov et al. 2007). At present, the only example of a system where a known planet creates an observed structure in a debris disk is the solar zodiacal cloud. Observations of other known planet-disk interactions will provide a direct test for the predictions made by our models.

A number of models have attempted to include collisions in dynamical calculations (e.g., Kenyon & Bromley 2005; Thébault & Augereau 2007), but few have been able to treat both collisional effects and resonant trapping simultaneously. This problem will likely yield to a statistical treatment of collisions (e.g., Thébault, Augereau & Beust 2003; Krivov et al. 2007). Several recent codes show promise in solving this issue (e.g., Grigorieva, Artymowicz & Thébault 2007), and dynamical disk models that self-consistently treat collisions are expected to emerge in the next few years.

Extremely Large Telescopes

The next generation of telescopes, including the TMT, GMT, and E-ELT, potentially can reach much fainter photometric sensitivity limits than KI and LBTI by having significantly more collecting area and suitable diameter to resolve the habitable zones of most stars likely to be in a sample for detection of an Earth-like exoplanet. If the telescopes are optimized for performance in the thermal infrared, it is possible that many lower mass stars could be searched for debris disks than will be possible with KI and LBTI. For example, the GMT expected photometric sensitivity at N band in 1 hour is approximately 20 μJy. If the AO performance is similar to LBTI, this is sufficient to detect dust down to 3 times solar level for all stars within 10 pc earlier than K4V.

Scattered light imaging will also be a focus of ELTs with similar high-contrast AO systems to GPI and SPHERE (e.g., the Planet Formation Imager for the Thirty Meter Telescope; Macintosh et al. 2006). Based on current design studies, PFI will reach similar or very slightly greater contrast than GPI (an optical depth of 3×10^{-5}), but its improved inner working angle (0.03") will allow imaging inwards toward the habitable zone for many targets, and to scales comparable to our own asteroid belt (near the "snow line") for young systems as distant as Taurus.

An Exozodiacal Dust Mission

Given the challenging nature of detecting exozodiacal dust from the ground, and the importance of it for direct imaging, a mission to characterize exozodiacal dust explicitly is an attractive option. Such a mission might be carried out in the infrared, via detection of thermal emission, or in the visible via scattered light. In either case it will be critical to measure dust in the habitable zone, which requires observing dust at 1 AU or equivalent for stars of different luminosity. To do so likely requires a significant mission, on the scale of an

Exoplanet Exploration Probe, rather than a SMEX-scope mission, but the scope of such a mission should be further explored as a first step toward assessing its feasibility.

Several coronagraphic missions are currently under study as possible Probe class Exoplanet missions, including ACCESS and the Visible Light Nulling Coronagraph. A 2-m class coronagraph (Stapelfeldt et al. 2007) provides the 0.1 spatial resolution needed to resolve the rings, warps, and asymmetries driven by planetary perturbations in these disks. With contrast improved ~1000 times over *HST*, it also will be sensitive enough to detect zodiacal disks at approximately solar level, enabling comparative studies of dust inventory and properties across stellar ages and spectral types.

An infrared mission that can observe all the nearby stars of interest to the flagship Darwin and TPF missions has been under study for many years, and is called the Fourier-Kelvin Stellar Interferometer (FKSI) mission (Danchi et al. 2003). The present design is a passively cooled structurally connected interferometer, operating at 60 K, from 3–8 (or 10) μm, with two 50-cm apertures separated by 12.5 m on a boom. This system has been extensively studied in the context of detecting and characterizing debris disks (see Defrère et al. 2008) and has been shown to be able to detect, within a few minutes, 1 Solar System zodi disks in the habitable zone of any star within 30 pc that is accessible within its field of regard (FoR). With a sunshade having a ±20-degree FoR a survey of 443 stars (28 F, 74 G, 164 K, and 177 M stars), and this number goes up to > 900 stars if the FoR is increased to ±40 degrees. Thus, an infrared space interferometer is not limited in spectral types or the number of stars that can be surveyed, except by its sunshade configuration. Further details on a small structurally connected interferometer are discussed in Chapter 4 in this volume.

5.4 Research & Analysis Goals

Furthering knowledge of the existence, prevalence, and strength of eoxozodiacal dust disks is critical for planning of future direct-imaging missions for Earth-like exoplanets. The development of a Design Reference Mission for any of the direct-imaging missions under consideration, including TPF-C, TPF-O, or TPF-I, requires information about the average zodiacal dust density around target stars. The information gleaned from detection of exozodiacal dust may also enhance our understanding of exoplanetary systems, as has already happened with observations from *HST* and *Spitzer*. The prevalence of dust in the habitable zones, and the structure of this dust, can provide important clues to the architectures of exoplanetary systems. The pivotal nature of this information leads us to the following three recommendations.

- Since information about dust in the habitable zone is crucial to planning future direct detection missions, the continued support of KI, LBTI, as well as any additional efforts that can address this question is needed to maintain momentum in this area.
- Exoplanet Probe class missions that can address the density and distribution of dust in other planetary systems should be further studied in order to optimize their scientific return and cost and technical feasibility. An Exoplanet Probe mission to detect and characterize debris disks and circumstellar material around all TPF and Darwin target stars, and to detect and characterize the atmospheres of Super Earth to giants will reduce scientific and technical risk for later flagship missions.

- A robust theory program and development of collisional debris disk models will aid in decoding the resonant structures induced by planets in observed debris disks. These models will give insight into dust transport and the detectability of exoplanets via observations of disk structure.

5.5 Contributors

Olivier Absil, LAOG

Rachel Akeson, NASA Exoplanet Science Institute, Caltech

David Ardila, Spitzer Science Center

James Breckenridge, Jet Propulsion Laboratory

Geoffrey Bryden, Jet Propulsion Laboratory

Christine Chen, STScI

David Ciardi, NASA Exoplanet Science Institute, Caltech

Mark Clampin, NASA Goddard Space Flight Center

Vincent Coudé du Foresto, Observatoire de Paris

William Danchi, NASA Goddard Space Flight Center

Denis Defrère, Université de Liège

Dennis Ebbets, Ball Aerospace

Sally Heap, NASA Goddard Space Flight Center

John Krist, Jet Propulsion Laboratory

Marc Kuchner, NASA Goddard Space Flight Center

Charles Lillie, Northrop Grumman

Patrick Lowrance, Spitzer Science Center

Stanimir Metchev, UCLA

Rafael Millan-Gabet, NASA Exoplanet Science Institute, Caltech

Marshall Perrin, UCLA

Meyer Pesenson, Caltech

Peter Plavchan, NASA Exoplanet Science Institute, Caltech

Sam Ragland, Keck Observatory

Stephen Rinehart, NASA Goddard Space Flight Center

Aki Roberge, NASA Goddard Space Flight Center

Chris Stark, University of Maryland

Karl Stapelfeldt, Jet Propulsion Laboratory

Motohide Tamura, NAOJ

Angelle Tanner, Jet Propulsion Laboratory

Neal Turner, Jet Propulsion Laboratory/Caltech

Bruce Woodgate, NASA Goddard Space Flight Center

5.6 References

Absil, O., Di Folco, E., Mérand, A., et al. 2008, "A near-infrared interferometric survey of debris disc stars. II. CHARA/FLUOR observations of six early-type dwarfs," A&A, 487, 1041–1054

Absil, O., Di Folco, E., Mérand, A., et al. 2006, "Circumstellar material in the Vega inner system revealed by CHARA/FLUOR," A&A, 452, 237–244

Akeson, R., Ciardi, D. R., Millan-Gabet, R., et al. 2009, "Dust in the inner regions of debris disks around A stars," ApJ, 691, 1896–1908

Apai, D., Pascucci, I., Brandner, W., et al. 2004, "NACO polarimetric differential imaging of TW Hya. A sharp look at the closest T Tauri disk," A&A, 415, 671–676

Beichman, C. A., Bryden, G., Stapelfeldt, K. R, et al. 2006, "New Debris Disks around Nearby Main-Sequence Stars: Impact on the Direct Detection of Planets," ApJ, 652, 1674–1693

Beichman, C. A., Bryden, G., Gautier, T. N, et al. 2005, "An Excess Due to Small Grains around the Nearby K0 V Star HD 69830: Asteroid or Cometary Debris?" ApJ, 626, 1061

Brandeker, A., Liseau, R., Olofsson, G., et al. 2004, "The spatial structure of the β Pictoris gas disk," A&A, 413, 681

Brown, R. A. 2005, "Single-Visit Photometric and Obscurational Completeness," ApJ, 624, 1010

Butler, R. P., Vogt, S. S., Marcy, G. W., et al. 2004, "A Neptune-Mass Planet Orbiting the Nearby M Dwarf GJ 436," ApJ, 617, 580–588

Chauvin, G., Lagrange, A.-M., Dumas, C., et al. 2004, "A giant planet candidate near a young brown dwarf. Direct VLT/NACO observations using IR wavefront sensing," A&A, 425, L29–L32

Ciardi, D. R., van Belle, G. T., Akeson, R. L., Thompson, R. R., Lada, E. A., & Howell, S. B. 2001, "On the near-infrared size of Vega," ApJ, 559, 1147–1154

Clampin, M. 2007, "The James Webb Space Telescope (JWST): A Tool for the Study of Planetary System Formation and Evolution," American Astronomical Society Division of Planetary Sciences meeting #39, #12.05, Bull. Am. Astron. Soc., 39, 432.

Clampin, M., Krist, J. E., Ardilla, D. R., et al. 2003, "Hubble Space Telescope ACS Coronagraphic Imaging of the Circumstellar Disk around HD 141569A," AJ, 126, 385–392

Colavita, M. M., Serabyn, E., Wizinowich, P. L., et al. 2006, "Nulling at the Keck Interferometer," Proc. SPIE, 6268, 626803

Colavita, M. M., Serabyn, E., Booth, A. J., et al. 2008, "Keck Interferometer nuller update," Proc. SPIE, 7013, 70130A

Danchi, W. C., Deming, D., Kuchner, M. J., et al. 2003, "Detection of Close-In Extrasolar Giant Planets Using the Fourier-Kelvin Stellar Interferometer," ApJ, 597, 57

Defrère, D., Absil, O., Coudé du Foresto, V., Danchi, W. C., & den Hartog, R. 2008, "Nulling interferometry: performance comparison between space and ground-based sites for exozodiacal disc detection," A&A, 490, 435–455

Deller, A.T., & Maddison, S.T. 2005, "Numerical modelling of dusty debris disks," ApJ, 625, 398–413

Dermott, S. F., Jayaraman, S., Xu, Y. L., et al. 1994, "A circumsolar ring of asteroidal dust in resonant lock with the Earth," Nature, 369, 719–723

di Folco, E., Absil, O., Augereau, J.-C., et al. 2007, "A near-infrared interferometric survey of debris disk stars. I. Probing the hot dust content around ε Eridani and τ Ceti with CHARA/FLUOR," A&A, 475, 243–250

Dohnanyi, J. S. 1969, "Collisional models of asteroids and their debris," J. Geophys. Res., 74, 2531–2554

Doyon, R., Rowlands, N, Hutchings, J., et al. 2008, "The JWST tunable filter imager (TFI)," Proc. SPIE, 7010, 70100X

Fitzgerald, M. P., Kalas, P. G., Duchêne, G., et al. 2007, "The AU Microscopii Debris Disk: Multiwavelength Imaging and Modeling," ApJ, 670, 536–556

Gillett, F. C. & Mountain, M. 1998, "On the Comparative Performance of an 8-m NGST and a Ground Based 8-m Optical/IR Telescope," in *Science with the NGST*, edited by Smith, E. P., and Koratkar, A., ASP Conf. Ser., 133, 42

Golimowski, D. A., Ardilla, D. R., Krist, J. E., et al. 2006, "Hubble Space Telescope ACS Multiband Coronagraphic Imaging of the Debris Disk around β Pictoris," AJ, 131, 3109–3130

Gomes, R., Levison, H. F., Tsiganis, K., et al. 2005, "Origin of the cataclysmic Late Heavy Bombardment period of the terrestrial planets," Nature, 435, 466–469

Grady, C. A., Woodgate, B., Bruhweiler, F. C., et al. 1999, "Hubble Space Telescope Space Telescope Imaging Spectrograph Coronagraphic Imaging of the Herbig AE star AB Aurigae," ApJ, 523, L151–L154

Graham, J. R., Kalas, P. G., & Matthews, B. C. 2007, "The Signature of Primordial Grain Growth in the Polarized Light of the AU Microscopii Debris Disk," ApJ, 654, 595–605

Grigorieva, A., Artymowicz, P., & Thébault, Ph. 2007, "Collisional dust avalanches in debris discs," A&A, 461, 537–549

Heap, S. R., Lindler, D. J., Lanz, T. M., et al. 2000, "Space Telescope Imaging Spectrograph coronagraphic observations of β Pictoris," ApJ, 539, 435–444

Hillenbrand, L. A., Carpenter, J. M., Kim, J. S., et al. 2008, "The Complete Census of 70 μm-bright Debris Disks within the 'Formation and Evolution of Planetary Systems' Spitzer Legacy Survey of Sun-like Stars," ApJ, 677, 630–656

Hinz, P. M., Angel, J. R. P., Woolf, N. J., et al. 2000, "BLINC: a testbed for nulling interferometry in the thermal infrared," Proc. SPIE, 4006, 349

Hinz, P. M., Angel, J. R. P., Hoffmann, W. F., et al. 1998, "Imaging circumstellar environments with a nulling interferometer," Nature, 395, 251–253

Holland, W. S., Greaves, J. S., Dent, W. R. F., et al. 2003, "Submillimeter observations of an asymmetric dust disk around Fomalhaut," ApJ, 582, 1141–1146

Holweger, H., Hempel, M., van Thiel, T., et al. 1997, "The surface composition of β Pictoris," A&A, 320, L49–L52

Jackson, A. A., & Zook, H. A. 1989, "A Solar System dust ring with Earth as its shepherd," Nature, 337, 629–631

Johnson, J. A., Fischer, D. A, Marcy, G. W., et al. 2007, "Retired A Stars and Their Companions: Exoplanets Orbiting Three Intermediate-Mass Subgiants," ApJ, 665, 785–793

Kalas, P., Graham, J. R., Clampin, M. 2005, "A planetary system as the origin of structure in Fomalhaut's dust belt," Nature, 435, 1067

Kalas, P., Graham, J. R., Clampin, M. C., & Fitzgerald, M. P. 2006, "First Scattered Light Images of Debris Disks around HD 53143 and HD 139664," ApJ, 637, L57–L60

Kalas, P., Fitzgerald, M. P., & Graham, J. R. 2007, "Discovery of Extreme Asymmetry in the Debris Disk Surrounding HD 15115," ApJ, 661, L85–L88

Kenyon, S. J., & Bromley, B. C. 2005, "Prospects for Detection of Catastrophic Collisions in Debris Disks," AJ, 130, 269–279

Klahr, H., & Lin, D. N. C., "Dust distribution around HR4796A and HD141569: a self induced ring formation through a clumping instability," in *Protostars and Planets V*, Reipurth, B., Jewitt, D., and Keil, K., editors, (University of Arizona Press, Tucson, 2006), contribution No. 1286, 8361.pdf. http://www.lpi.usra.edu/meetings/ppv2005/pdf/8361.pdf

Krist, J., Beichman, C. A., Trauger, J. T., et al. 2007, "Hunting planets and observing disks with the JWST NIRCam coronagraph," Proc. SPIE, 6693, 66930H

Krist, J. E., Ardila, D. R., Golimowski, D. A., et al. 2005, "Hubble Space Telescope Advanced Camera for Surveys Coronagraphic Imaging of the AU Microscopii Debris Disk," AJ, 129, 1008–1017

Krivov, A. V., Queck, M., Lohne, T., et al. 2007, "On the nature of clumps in debris disks," A&A, 462, 199–210

Kuchner, M. J., & Holman, M. J. 2003 "The Geometry of Resonant Signatures in Debris Disks with Planets," ApJ, 588, 1110–1120

Lay, O. P., Martin, S. R., & Hunyadi S. L. 2007, "Planet-finding performance of the TPF-I Emma architecture," Proc. SPIE, 6693, 66930A

Liou, J. C., & Zook, H. A. 1999, "Signatures of the Giant Planets Imprinted on the Edgeworth-Kuiper Belt Dust Disk," AJ, 118, 580–590

Lisse, C. M., Beichman, C. A., Bryden, G., & Wyatt, M. C. 2007, "On the Nature of the Dust in the Debris Disk around HD 69830," ApJ, 658, 584–592

Liu, W. M., Hinz, P. M., Hoffmann, W. F., et al. 2004, "Adaptive Optics Nulling Interferometric Constraints on the Mid-Infrared Exozodiacal Dust Emission around Vega," ApJ, 610, 125

Macintosh B., Graham, J., Palmer, D., et al. 2006, "The Gemini Planet Imager," Proc. SPIE, 6272, 62720L

Metchev, S. A., Hillenbrand, L. A., & Meyer, M. R. 2004, "Ten Micron Observations of Nearby Young Stars," ApJ, 600, 435–450

Metchev, S. A., Eisner, J. A., Hillenbrand, L. A., & Wolf, S. 2005, "Adaptive Optics Imaging of the AU Microscopii Circumstellar Disk: Evidence for Dynamical Evolution," ApJ, 622, 451–462

Morbidelli, A., Levison, H. F., Tsiganis, K., et al. 2005, "Chaotic capture of Jupiter's Trojan asteroids in the early Solar System," Nature, 435, 462–465

Morbidelli, A., Chambers, J., Lunine, J. I., et al. 2000, "Source regions and time scales for the delivery of water to Earth," Meteoritics and Planetary Science, 35, 1309–1320

Moro-Martín, A., & Malhotra, R., 2002, "A Study of the Dynamics of Dust from the Kuiper Belt: Spatial Distribution and Spectral Energy Distribution," AJ, 124, 2305–2321

Olofsson, G., Liseau, R., Brandeker, A. 2001, "Widespread Atomic Gas Emission Reveals the Rotation of the β Pictoris Disk," ApJ, 563, 770

Perrin, M. D., Graham, J. R., Kalas, P., et al. 2004, "Laser Guide Star Adaptive Optics Imaging Polarimetry of Herbig Ae/Be Stars," Science, 303, 1345–1348

Pinte, C., Fouchet, L., Ménard, F., Gonzalez, J.-F., & Duchêne, G. 2007, "On the stratified dust distribution of the GG Tau circumbinary ring," A&A, 469, 963–971

Reche, R., Beust, H., Augereau, J.-C., et al. 2008, "On the observability of resonant structures in planetesimal disks due to planetary migration," A&A, 480, 551–561

Roberge, A., Feldman, P. D., Weinberger, A. J., et al. 2006, "Stabilization of the disk around β Pictoris by extremely carbon-rich gas," Nature, 441, 724–726

Schneider, G., Smith, B. A., Becklin, E. E., et al. 1999, "NICMOS Imaging of the HR 4796A Circumstellar Disk," ApJ, 513, L127–L130

Serabyn, E., Booth, A. J., Colavita, M. M. 2004, "The Keck interferometer nuller: system architecture and laboratory performance," Proc. SPIE, 5491, 806

Stapelfeldt, K. R., Holmes, E. K., Chen, C., et al. 2004, "First Look at the Fomalhaut Debris Disk with the Spitzer Space Telescope," ApJ Sup. Ser., 154, 458–462

Stapelfeldt, K. R., Trauger, J., Traub, W., et al. 2007, "First Steps in Direct Imaging of Planetary Systems like our Own: The Science Potential of 2-m Class Optical Space Telescope," Whitepaper submitted to the AAAC Exoplanet Task Force, arXiv:0707.1886

Stark, C. C. & Kuchner, M. J. 2008, "The Detectability of Exo-Earths and Super-Earths Via Resonant Signatures in Exozodiacal Clouds," ApJ, 686, 637–648

Takeuchi, T., & Artymowicz, P. 2001, "Dust migration and morphology in optically thin circumstellar disks," ApJ, 557, 990–1006

Thébault, P., & Augereau, J.-C. 2007, "Collisional Processes and Size Distribution in Spatially Extended Debris Discs," A&A, 472, 169–185

Thébault, P., Augereau, J. C., & Beust, H. 2003, "Dust production from collisions in extrasolar planetary systems. The inner beta Pictoris disc," A&A, 408, 775–788

Thi, W.-F., van Dishoeck, E. F., Blake, G. A., et al. 2000, "H_2 and CO Emission from Disks around T Tauri and Herbig Ae Pre-Main-Sequence Stars and from Debris Disks around Young Stars: Warm and Cold Circumstellar Gas," ApJ, 561, 1074–1094

Trilling, D. E., Bryden, G, Beichman, C. A., et al. 2008, "Debris Disks around Sun-like Stars," ApJ, 674, 1086–1105

Tsiganis, K., Gomes, R., Morbidelli, A., et al. 2005, "Origin of the orbital architecture of the giant planets of the Solar System," Nature, 435, 459–461

Wallner, O., Ergenzinger, K., Johann, U. 2008, "Terrestrial exo-planet science by nulling interferometry: instrument design and scientific performance," Proc. SPIE, 7013, 70132O

Wilner, D. J., Holman, M. J., Kuchner, M. J., et al. 2002, "Structure in the Dusty Debris around Vega," ApJ, 569, L115–L119

Wolszczan, A., & Frail, D. A. 1992, "A Planetary System around the Millisecond Pulsar PSR 1257+12," Nature, 355, 145–147

Wyatt, M. C. 2003, "Resonant Trapping of Planetesimals by Planet Migration: Debris Disk Clumps and Vega's Similarity to the Solar System," ApJ, 598, 1321–1340

Wyatt, M. C., 2005, "The insignificance of P-R drag in detectable extrasolar planetesimal belts," A&A, 433, 1007–1012

Wyatt, M. C., 2006, "Dust in Resonant Extrasolar Kuiper Belts: Grain Size and Wavelength Dependence of Disk Structure," ApJ, 639, 1153–1165

Zuckerman, B., & Song, I. 2004, "Young Stars Near the Sun," ARA&A, 42, 685–721